

CCD BV and 2MASS photometric study of the open cluster NGC 1513

S. Bilir¹ • T. Güver² • I. Khamitov³ • T. Ak^{1,3} •
S. Ak¹ • K. B. Coşkunoglu¹ • E. Paunzen¹ •
E. Yaz¹

© Springer-Verlag ●●●●

Abstract We present CCD BV and JHK_s 2MASS photometric data for the open cluster NGC 1513. We observed 609 stars in the direction of the cluster up to a limiting magnitude of $V \sim 19$ mag. The star count method shows that the centre of the cluster lies at $\alpha_{2000} = 04^h09^m36^s$, $\delta_{2000} = 49^\circ28'43''$ and its angular size is $r = 10$ arcmin. The optical and near-infrared two-colour diagrams reveal the colour excesses in the

direction of the cluster as $E(B - V) = 0.68 \pm 0.06$, $E(J - H) = 0.21 \pm 0.02$ and $E(J - K_s) = 0.33 \pm 0.04$ mag. These results are consistent with normal interstellar extinction values. Optical and near-infrared Zero Age Main-Sequences (ZAMS) provided an average distance modulus of $(m - M)_0 = 10.80 \pm 0.13$ mag, which can be translated into a distance of 1440 ± 80 pc. Finally, using Padova isochrones we determined the metallicity and age of the cluster as $Z = 0.015 \pm 0.004$ ($[M/H] = -0.10 \pm 0.10$ dex) and $\log(t/yr) = 8.40 \pm 0.04$, respectively.

S. Bilir

¹Istanbul University, Faculty of Science, Department of Astronomy and Space Sciences, 34119 University, Istanbul, Turkey

T. Güver

²University of Arizona, Department of Astronomy, 933 N. Cherry Ave., Tucson, AZ 85721

I. Khamitov

³TÜBİTAK National Observatory, Akdeniz University Campus, 07058 Antalya, Turkey

T. Ak

¹Istanbul University, Faculty of Science, Department of Astronomy and Space Sciences, 34119 University, Istanbul, Turkey

³TÜBİTAK National Observatory, Akdeniz University Campus, 07058 Antalya, Turkey

S. Ak

¹Istanbul University, Faculty of Science, Department of Astronomy and Space Sciences, 34119 University, Istanbul, Turkey

K. B. Coşkunoglu

¹Istanbul University, Faculty of Science, Department of Astronomy and Space Sciences, 34119 University, Istanbul, Turkey

E. Paunzen

⁴Institut für Astronomie der Universität Wien, Türkenschanzstr. 17, 1180 Wien, Austria

E. Yaz

¹Istanbul University, Faculty of Science, Department of Astronomy and Space Sciences, 34119 University, Istanbul, Turkey

Keywords Galaxy: Open Cluster and associations: individual: NGC 1513 stars: interstellar extinction

1 Introduction

Systematic studies of open clusters help understand the galactic structure and star formation processes as well as stellar evolution. By utilizing colour-magnitude diagrams of the stars observed in the optical/near-infrared (NIR) bands, it is possible to determine the underlying properties of open clusters such as age, metal abundance and distance. In this study, we continue this effort by analyzing the optical and NIR data of the open cluster NGC 1513.

The young open cluster NGC 1513 = C 0406+493 ($\alpha_{2000} = 04^h09^m10^s$, $\delta_{2000} = 49^\circ31'00''$, $l = 152^\circ.50$, $b = -1^\circ.66$) is classified as a Trümpler class II 1m, a moderately rich cluster with a low central concentration. NGC 1513 was first studied astrometrically by Bronnikova (1958a) who determined the proper motions using a single pair of plates with an epoch difference of 55 years. Barhatova & Drjakhlushina (1960) published photographic and photovisual magnitudes of 49 stars from Bronnikova's (1958b) list.

Del Rio & Huestamendia (1988) obtained the first photoelectric UBV magnitudes of 31 stars and photographic RGU magnitudes for 116 stars in the cluster region. They determined colour excess, distance and the age of the cluster from RGU data as $E(G - R) = 0.93$ mag, 1320 pc and $\log(t/yr) = 8.18$, respectively. To test stellar evolution models, Frandsen & Arentoft (1998) studied NGC 1513 using BV photometry. Frolov et al. (2002) studied the astrometric data-sets of 333 stars in the direction of the cluster, and showed that 33 of those stars are most probably cluster members. Using BV photometric data, they also determined the cluster's metal abundance to be about solar metallicity and its age as $\log(t/yr) = 8.40$. Maciejewski & Niedzielski (2007) studied 42 open clusters using CCD BV photometry and obtained the structural and astrophysical parameters for NGC 1513. According to their measurements the cluster's colour excess, distance modulus and age are $E(B - V) = 0.76$ mag, $(m - M) = 12.96$ mag and $\log(t/yr) = 7.4$, respectively.

In this study we observed the open cluster NGC 1513 with BV filters, and matched our results with 2MASS photometry. We determined the colour excesses in optical and near-infrared region. Then, we used optical and near-infrared data to obtain the cluster's distance modulus, metal abundance and age.

The paper is organized as follows. We present the observations and data reductions in Section 2, while in Section 3, we describe the data analysis. Finally, Section 4 contains the conclusions of our study.

2 Observations and Data Reduction

2.1 Optical Data

CCD BV photometric observations of NGC 1513 were made in 8th and 9th of October 2004 at the TÜBİTAK National Observatory (TUG) using the 1.5-m Russian-Turkish Telescope RTT150 and ANDOR DW436 CCD camera (back illuminated, 2k×2k pixels, 13.5×13.5 μm). The resulting image on the CCD has a field of view of $8' \times 8'$. Since the spatial diameter of NGC 1513 is approximately $15' \times 15'$ we divided the field into four equal subfields and created a mosaic image from these. Coordinates of the subfields and observation summary are given in Table 1 and the subfields are shown in Fig. 1.

For each subfield we obtained six images in B and V bands, which are then combined for each filter and median images are used for further analysis. Obtained images were reduced using the computing facilities avail-

able at TUG, Turkey. The standard IRAF¹ routines were utilized for prereduction, and the IRAF version of the DAOPHOT package (Stetson 1987, 1992) was used with a quadratically varying point spread function (PSF) to derive positions and magnitudes for the stars. To determine the PSF, we used several well-isolated stars in the entire frame. Output catalogues for each frame were aligned in position and magnitude, and final (instrumental) magnitudes were computed as weighted averages of the individual values. Magnitudes of the stars brighter than $V = 10$ could not be measured due to saturation of the detector pixels.

The instrumental b and v magnitudes were transformed into standard Johnson B and V magnitudes using fitting coefficients derived from observations of the standard field stars whose magnitudes were given by Del Rio & Huestamendia (1988) and Frandsen & Arentoft (1998) for photoelectric UBV and CCD UBV photometry, and taking airmass corrections into account. 15 and 16 standard stars given by Del Rio & Huestamendia (1988) and Frandsen & Arentoft (1998) have a magnitude and colour range of $12 < V < 18$ and $0.55 < B - V < 1.70$ mag. Errors of magnitude and colours for those stars are given as ± 0.02 and ± 0.01 for V and B-V, respectively (Del Rio & Huestamendia 1988; Frandsen & Arentoft 1998). Due to our subfield selection, we had 8-11 standard stars in each field. We then used these standard stars to estimate the standard magnitude of the other stars in the field.

The magnitude and colour differences between our values and Del Rio & Huestamendia (1988) and Frandsen & Arentoft (1998) are shown in Fig. 2. The mean magnitude and colour differences and their respective standard deviations are 0.005, -0.011 and 0.07, 0.07 mag.

The internal errors, as derived from DAOPHOT, in magnitude and colour are plotted against V magnitude in Fig. 3 and the mean values of the errors are listed in Table 2. Figure 3 shows that photometric error is ≤ 0.015 mag at $V \sim 19$ mag while the colour error is 0.024 mag.

We compared our results with a recent BV photometric study on NGC 1513, performed by Maciejewski & Niedzielski (2007). 452 out of 609 stars in our sample matched with Maciejewski & Niedzielski's (2007). The magnitude and colour differences between our results and those of Maciejewski & Niedzielski (2007) are given in Fig. 4. As seen from Fig. 4a the zero point of the magnitude difference is at $\Delta V = -0.05$ mag. The trend seen in Fig. 4b indicates a disagreement between our values and Maciejewski & Niedzielski's (2007). After

¹<http://iraf.noao.edu>

Table 1 Coordinates of the subfields and log of observations with dates, airmass and exposure times for each filter. Exposure times are given in seconds.

Sub-field	α_{2000}	δ_{2000}	Exposure	B Band		V Band		
				Date	Airmass	Exposure	Date	Airmass
F1	04 10 10	+49 33 20	30×3	10/09/2004	1.036	10×3	10/08/2004	1.257
F1	04 10 10	+49 33 20	600×3	10/09/2004	1.030	30×3	10/08/2004	1.228
F2	04 09 32	+49 33 20	30×3	10/09/2004	1.025	10×3	10/08/2004	1.188
F2	04 09 32	+49 33 20	600×3	10/09/2004	1.026	30×3	10/08/2004	1.168
F3	04 10 10	+49 27 15	30×3	10/09/2004	1.089	10×3	10/08/2004	1.091
F3	04 10 10	+49 27 15	600×3	10/09/2004	1.063	30×3	10/08/2004	1.079
F4	04 09 32	+49 27 15	30×3	10/09/2004	1.097	10×3	10/08/2004	1.137
F4	04 09 32	+49 27 15	600×3	10/09/2004	1.037	30×3	10/08/2004	1.121

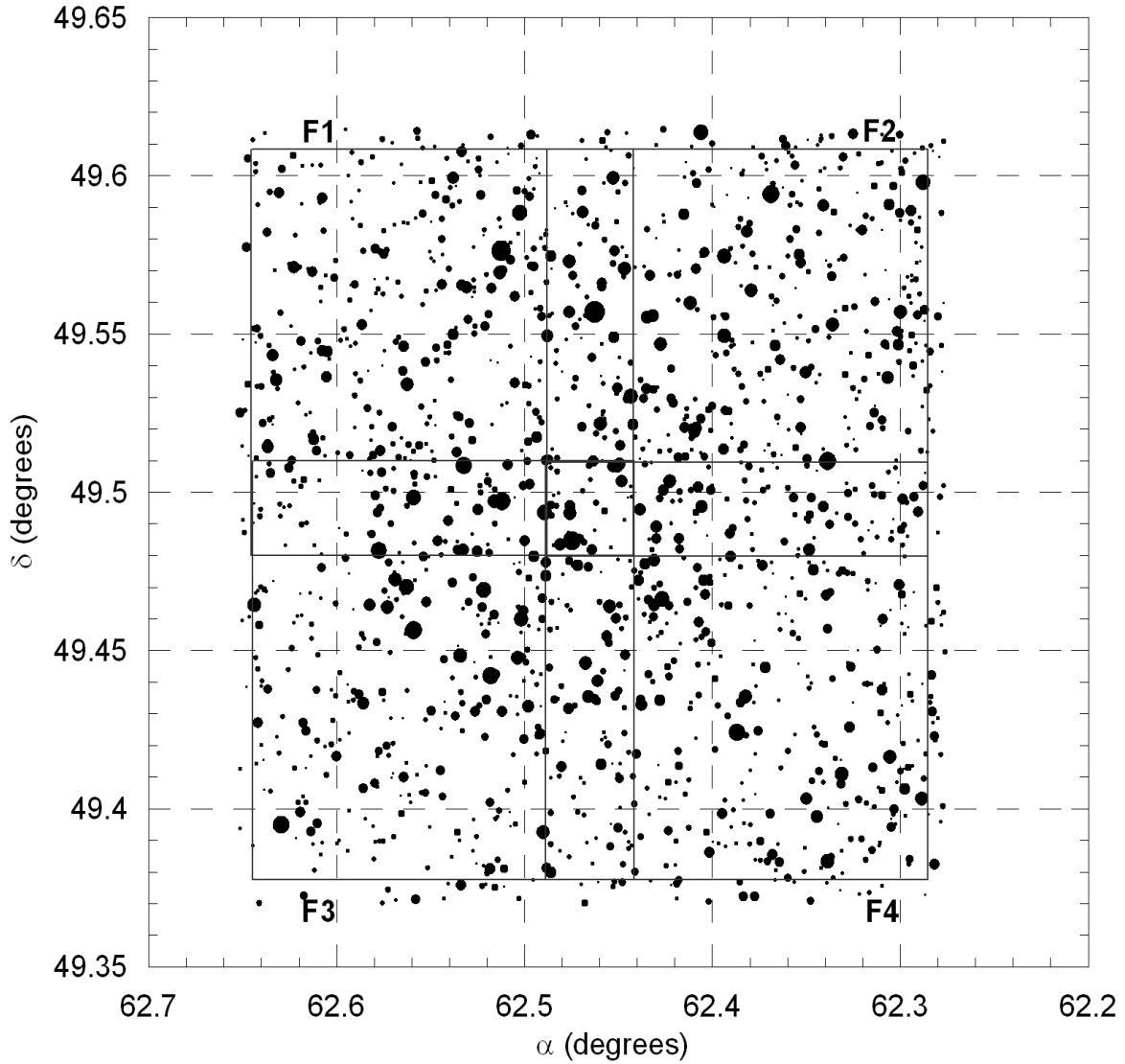


Fig. 1 Finding chart of the stars in the field of NGC 1513. Four subfields (F1, F2, F3 and F4) were also shown. Filled circles of different sizes represent brightness of the stars. Smallest size denotes stars of $V \sim 19$ mag.

Table 2 Mean photometric errors and number of stars in optical and near-infrared magnitudes and colours for different magnitude intervals. N is the number of the stars for each interval.

V (mag)	σ_V (mag)	σ_{B-V} (mag)	N_{BV}	σ_J (mag)	σ_{J-H} (mag)	σ_{J-K_s} (mag)	N_{2MASS}
(10,11]	0.001	0.001	1	0.024	0.037	0.033	1
(11,12]	0.001	0.001	7	0.023	0.036	0.031	7
(12,13]	0.001	0.001	9	0.024	0.038	0.033	9
(13,14]	0.001	0.001	32	0.026	0.041	0.036	32
(14,15]	0.001	0.001	58	0.026	0.041	0.037	58
(15,16]	0.002	0.003	70	0.027	0.043	0.040	70
(16,17]	0.003	0.005	105	0.032	0.051	0.051	105
(17,18]	0.005	0.009	133	0.038	0.060	0.067	133
(18,19]	0.009	0.016	194	0.056	0.087	0.109	191

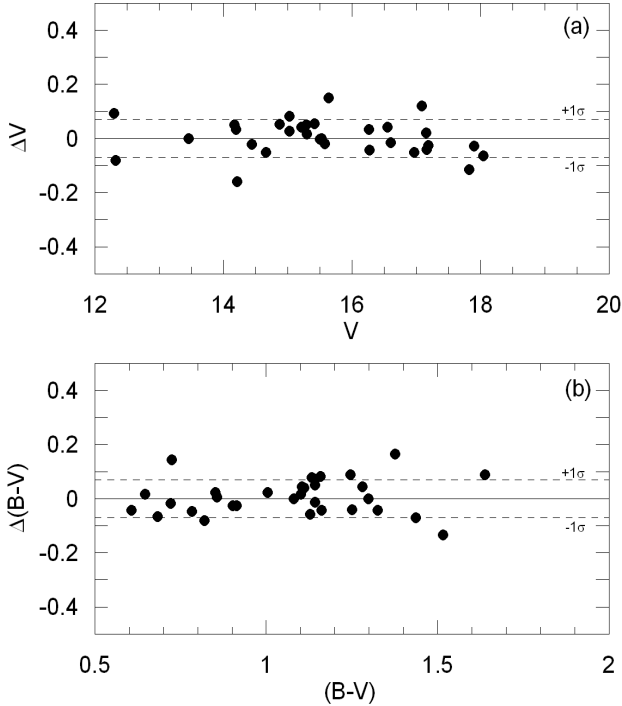


Fig. 2 Magnitude (a) and colour (b) differences between the values calculated in this study and Del Rio & Huestamendia's (1988) and Frandsen & Arentoft's (1998). V and $(B - V)$ represent the magnitudes and colours obtained in this study. The dashed lines denote $\pm 1\sigma$.

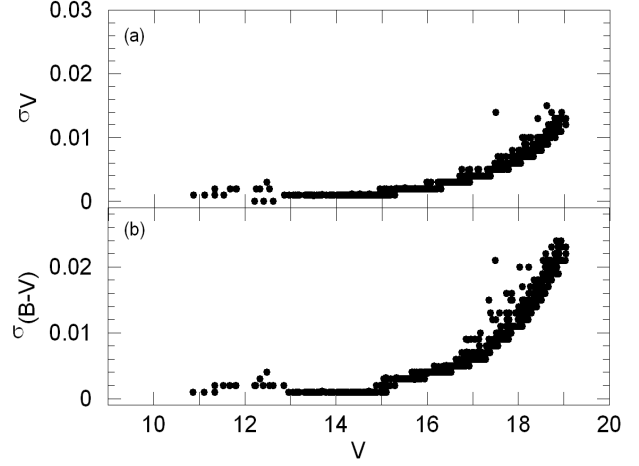


Fig. 3 Photometric errors (in magnitude) corresponding to the brightness measurement at V and $(B - V)$ are plotted against the V -band brightness. Error on the y-axis represent the internal errors as estimated by DAOPHOT routine.

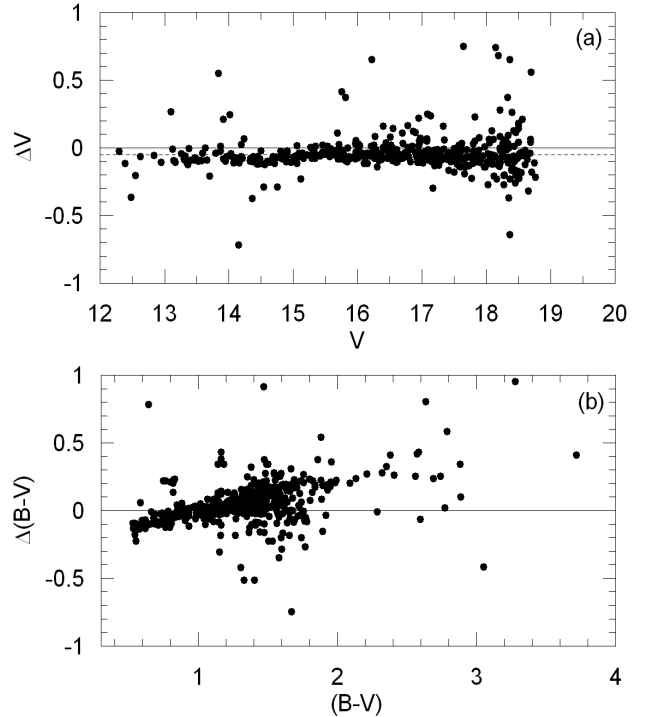


Fig. 4 Magnitude (a) and colour (b) differences between the values measured in this study and Maciejewski & Niedzielski's (2007) values. V and $(B - V)$ represent the magnitudes and colours obtained in this study. The dashed line in panel (a) denotes $\Delta V = -0.05$ mag.

analyzing and comparing our data with previous studies, we conclude that our values are not in agreement with values given by Maciejewski & Niedzielski (2007). This discrepancy in Fig. 4 might exist because of the fact that Maciejewski & Niedzielski (2007) did not pick standard stars from a large magnitude and colour interval.

2.2 Near-Infrared Data

The near-infrared JHK_s photometric data were taken from the digital Two Micron All-sky Survey² (2MASS). 2MASS uniformly scanned the entire sky in three near-infrared bands J ($1.25\mu\text{m}$), H ($1.65\mu\text{m}$) and K_s ($2.17\mu\text{m}$) with two highly automated 1.3-m telescopes equipped with a three-channel camera, where each channel consists of a 256×256 array of HgCdTe detectors. The photometric uncertainty of the data is less than 0.155 at $K_s \sim 16.5$ magnitude which is the photometric completeness of 2MASS for stars with $|b| > 25^\circ$ (Skrutskie et al. 2006). We picked stars in a field, of size 25 arcmin^2 , in the direction of NGC 1513 from Cutri et al.’s Point Source Catalogue (2003) and calculated the limiting magnitudes and photometric errors are $J = 16.5 \pm 0.125$, $H = 16.0 \pm 0.143$, $K_s = 15.5 \pm 0.175$ mag. These photometric errors are in agreement with the error values given for high latitude star fields.

We detected 609 stars in BV photometry in our observations. We then compared our results with Cutri et al.’s Point Source Catalogue (2003) and matched the appropriate stars. After that, we obtained the 2MASS magnitudes for the 606 observed stars. 534 out of these 606 stars have a “AAA” quality flag, which means the signal noise ratio is $SNR \geq 10$, i.e. they have the highest quality measurements. The 2MASS magnitude and colour errors are as follows: $0.018 \leq \sigma_J \leq 0.145$, $0.032 \leq \sigma_{J-H} \leq 0.232$ and $0.030 \leq \sigma_{J-K_s} \leq 0.241$ mag. Errors are given in Table 2 and shown in Fig. 5. Table 2 reveals that the accuracy of optical data is better than near-infrared data, because there are more observations in the former. The coordinates, optical and near-infrared magnitudes and their errors for 609 observed stars are given in Table 3.

3 Data Analysis

3.1 Cluster’s Centre and Radial Density Profile

NGC 1513 is a cluster with low central concentration. The centre of the cluster can only be determined roughly by eye-estimation. To determine the

centre more precisely, we applied the star-count method and divided the cluster into one arcmin sized squares. We then calculated the surface distributions of those squares (Fig. 6). We assumed the centre of the cluster as the square’s centre with maximum star density. The star symbol seen in Fig. 6 indicates the centre of the cluster with equatorial coordinates $\alpha_{2000} = 04^h 09^m 36^s$, $\delta_{2000} = 49^\circ 28' 43''$ and galactic coordinates $l = 152^\circ.57$, $b = -1^\circ.64$. This result is in agreement with Maciejewski & Niedzielski’s (2007) $\alpha_{2000} = 04^h 09^m 46^s$, $\delta_{2000} = 49^\circ 28' 28''$, but somewhat different than Frolov et al.’s (2002) $\alpha_{2000} = 04^h 10^m 38^s$, $\delta_{2000} = 49^\circ 31' 00''$ central equatorial coordinates. Considering our results were obtained from both optical and near-infrared photometric systems, we can state that our central coordinates are more accurate.

To establish the radial density profile we counted the stars with distances $r \leq 1$ arcmin from the centre of the cluster. We repeated this process up to $r = 15$ with 1 arcmin steps. The next step was to subtract the stars in previous areas from the later ones, so that we obtained only the amount of the stars within the relevant area, not a cumulative count. Finally, we divided the star counts in 15 fields by the appropriate areas, i.e. the areas of the fields those stars belong to. The density uncertainties in each field was calculated using Poisson noise statistics.

Using photometric data we plotted the radial density versus angular separation from the cluster’s centre in Fig. 6. The figure shows the radial density profile from the centre of the cluster to a maximum angular separation of 15 arcmin. The density shows a maximum at the centre $\rho = 8.5$ stars/arcmin² and then decreases down to $\rho = 5.5$ stars/arcmin² at 15 arcmin. The decrease becomes asymptotical at $r \sim 10$ arcmin, after that point there are a few cluster stars. To determine the structural parameters of the cluster more precisely, we applied the empirical King model (King 1966). The King model parameterizes the density function $\rho(r)$ as:

$$\rho(r) = f_{bg} + \frac{f_0}{1 + (r/r_c)^2}, \quad (1)$$

where f_{bg} , f_0 and r_c are background and central star densities and the core radius of the cluster, respectively. Fig. 6 reveals the background star density $f_{bg} = 5.5$ stars/arcmin². We then compared observational values with the ones we obtained from King profile using minimum χ^2 statistics. The analysis shows that $f_0 = 3.00 \pm 0.31$ stars/arcmin² and $r_c = 3.98 \pm 0.55$ arcmin. The degree of freedom of the analysis (dof) is 0.11, while its squared correlation coefficient (R^2) is 0.89. In Fig. 6, the dots stand for the observational

²<http://www.ipac.caltech.edu/2MASS/>

Table 3 The coordinates, optical and near-infrared magnitudes and their errors for 609 observed stars. The catalogue containing this information can be obtained electronically.

ID	α_{2000} (hh:mm:ss)	δ_{2000} (dd:mm:ss)	B (mag)	B_{err} (mag)	V (mag)	V_{err} (mag)	J (mag)	J_{err} (mag)	H (mag)	H_{err} (mag)	K_s (mag)	$K_{s_{err}}$ (mag)
001	04:09:05.16	49:30:07.62	17.849	0.004	16.563	0.003	13.859	0.031	13.440	0.036	13.257	0.032
002	04:09:05.17	49:29:11.57	20.053	0.014	18.510	0.009	15.487	0.050	14.897	0.066	14.727	0.100
003	04:09:05.45	49:32:29.04	19.473	0.010	18.108	0.007	15.384	0.055	15.065	0.071	14.627	0.086
004	04:09:05.72	49:25:47.56	18.853	0.006	17.446	0.005	14.780	0.045	14.402	0.049	14.201	0.075
005	04:09:05.87	49:24:24.37	19.812	0.007	17.553	0.005	15.483	0.113	15.040	0.090	14.826	0.134
...
...
...
605	04:10:29.69	49:30:37.04	18.652	0.005	16.921	0.003	13.892	0.029	13.158	0.036	12.952	0.030
606	04:10:29.72	49:27:03.29	19.860	0.010	18.271	0.007	15.137	0.048	14.562	0.057	14.503	0.080
607	04:10:30.08	49:30:28.02	16.268	0.002	15.115	0.001	13.495	0.027	13.192	0.032	13.134	0.035
608	04:10:31.19	49:23:41.85	20.263	0.004	16.545	0.003	10.005	0.024	8.608	0.031	8.195	0.023
609	04:10:32.86	49:26:16.21	17.559	0.003	16.452	0.003	13.824	0.026	13.527	0.032	13.309	0.036

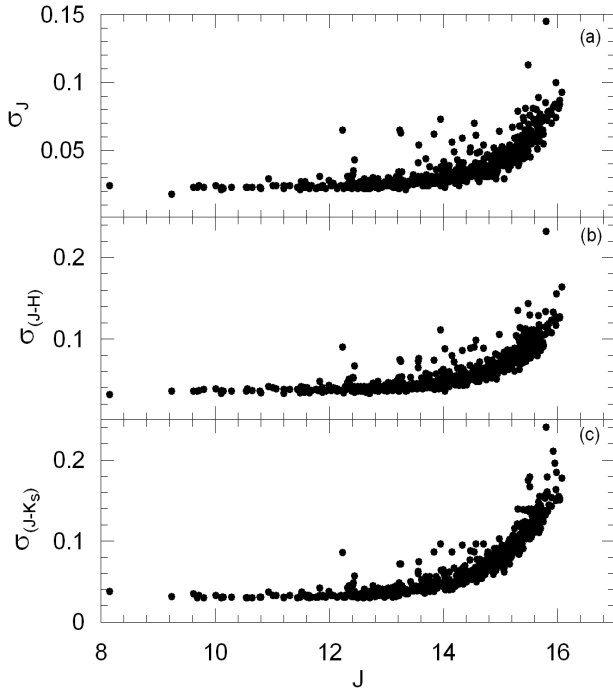


Fig. 5 Photometric errors (in magnitude) corresponding to the brightness measurement at J , $(J - H)$ and $(J - K_s)$ are plotted against the J -band brightness.

density values, whereas solid line represents the King profile. The error bars denote the Poisson errors in observations.

Maciejewski & Niedzielski (2007) analyzed the structural parameters of 42 open clusters using King model (King 1966). They obtained the parameters for NGC 1513 as: $r_{lim} = 9.2$, $r_c = 3.7$ arcmin, $f_0 = 2.47$ and $f_{bg} = 1.04$ stars/arcmin². Comparing our results with Maciejewski & Niedzielski's (2007) we can conclude that although the limiting radii and the core radii are in agreement, the central and background star densities somewhat differ.

To check our background central density value, we used the Besançon Galaxy model³ (Robin et al. 2003). We assumed the size of the field as 0.05 deg², and the magnitude range as $10 < V < 19$. We took colour excess $E(B - V) = 0.68$ and distance modulus values $(V - M_V) = 12.95$ mag from Sections 3.3 and 3.4. According to Besançon model there are 3.6 field stars per arcmin², which we showed as the dashed horizontal line in Fig. 6. At the core radius $r_c = 3.98$ arcmin, which we obtained for the cluster using King model (King 1966), the background star density is $\rho = 5.5$ stars/arcmin². This value differs slightly from Besançon model's 3.6 stars/arcmin². The observational and model background star densities are not in total agreement; there is a difference of 1.9 stars/arcmin². This discrepancy originates from the galactic model parameters, because Galaxy models use several parameters with fixed values for the entire Galaxy. However, Bilir et al. (2008) showed that galactic model parameters are a function

³<http://model.obs-besancon.fr/>

of absolute magnitude, galactic latitude and longitude, i.e. they do not have fixed values. This means models using fixed galactic model parameters can not always be used to explain observational data in different directions of the Galaxy.

Consequently, the analyses in this section show that the equatorial and galactic coordinates of the centre are $\alpha_{2000} = 04^h 09^m 36^s$, $\delta_{2000} = 49^\circ 28' 43''$ and $l = 152^\circ .57$, $b = -1^\circ .64$, respectively, and that the cluster has an angular radius of approximately 10 arcmin.

3.2 Colour-Magnitude Diagrams

We established optical and near-infrared colour magnitude diagrams (CMDs) for NGC 1513. In Fig. 7 we present $(B - V)/V$, $(J - H)/J$ and $(J - K_s)/K_s$ diagrams for NGC 1513. Since the central concentration of the cluster is relatively low, the determination of whether if a star is a field star or a member of the cluster using radial stellar density profile is tough. Even though we calculated the core radius of the cluster as $r_c = 3.98$ arcmin from Fig. 6, to determine cluster members with even more probability we chose the stars within the circle with radius $r = 5$ arcmin. By doing that, we obtained a more precise main-sequence in the CM diagram, which contains 343 stars in our sample. All of these 343 main-sequence stars are found in-between the two dashed lines in Fig. 7a-c. However, there are 110 more stars in-between the dashed lines with $5 < r \leq 15$ arcmin. This means the contamination in Fig. 7 is about 24 %.

However, Frolov et al.'s (2002) astrometric study regarding 333 stars in the direction of the cluster provides us information about cluster membership of the 609 observed stars. The filled and open circles in Fig. 7 represent Frolov et al.'s (2002) probable cluster members ($p > 50\%$) and other observed stars, respectively. The reason we use the probable cluster members is to decide which isochrone to use when determining the age of the cluster. The problem with the astrometrically determined high probability stars is that they can only be detected in brighter magnitudes. As seen in the CM diagrams in Fig. 7, there are a few giants in the direction of the cluster. The cluster membership probability of stars with numbers 360 and 380, which appear in the giant regions of the CMDs, are 90% and 93% (Frolov et al., 2002) according to their proper motion studies, respectively. Since there are no spectroscopic studies regarding these systems, it is unknown if these stars are giants or main-sequence stars. Recently, a new method was suggested by Bilir et al. (2006) to separate field giants from field dwarfs. This new method is based on the comparison of the 2MASS J , H , K_s with the V

magnitudes down to the limiting magnitude of $V = 16$ mag. The calibration equations used in separating giants from dwarfs are as follows:

$$J_0 = 0.957 \times V_0 - 1.079, \quad (2)$$

$$H_0 = 0.931 \times V_0 - 1.240, \quad (3)$$

$$(K_s)_0 = 0.927 \times V_0 - 1.292, \quad (4)$$

where “0” index denotes the de-reddened magnitudes. To apply this method, magnitudes of stars should be de-reddened. The colour excesses and the de-reddening method are given in detail in Section 3.3. The calibration and the de-reddened V_0 , J_0 , H_0 , $(K_s)_0$ magnitudes of the two stars were shown in Fig. 8. The de-reddening procedure is explained in detail in the next section. As seen from the Fig. 8 the stars appear to the right of the calibration lines, which means they are in the giant region. These two stars are cluster members astrometrically and giant stars photometrically. According to Pickles (1998) synthetic data the giant stars numbered 360 and 380 belong to K1 and K0 spectral types, respectively.

By selecting the stars within the circle with radius $r = 5$ arcmin and using Frolov et al.'s (2002) high probability member stars we determined a more precise main-sequence, which is an important factor in deciding the distance modulus of the cluster. By making this selection, we made a precise determination of the cluster's main-sequence's turn-off point which is the best age indicator.

3.3 Two Colour Diagrams and Colour Excesses

We present optical and near-infrared two-colour diagrams for $r \leq 5$ arcmin in Fig. 9. In Fig. 9a, we plotted $(J - H)_0$ versus $(B - V)_0$ whereas in Fig. 9b the axes are $(J - K_s)_0$ and $(B - V)_0$. Namely, we plotted a near-infrared colour versus an optical colour in each panel. To determine the reddening in the direction of the cluster we made use of the synthetic library of Pickles (1998). In Pickles' (1998) library we selected the metallicity to be $[M/H] = 0$ dex and main-sequence stars of different spectral types and obtained datasets for $(B - V)$, $(V - J)$, $(V - H)$, $(V - K)$. Since Pickles' near-infrared data are in Johnson's system, we used Carpenter's (2001) transformation equations (A1, A2, A3, A4) to obtain magnitudes of 2MASS bands (Table 4). We plotted the standard main-sequence from Table

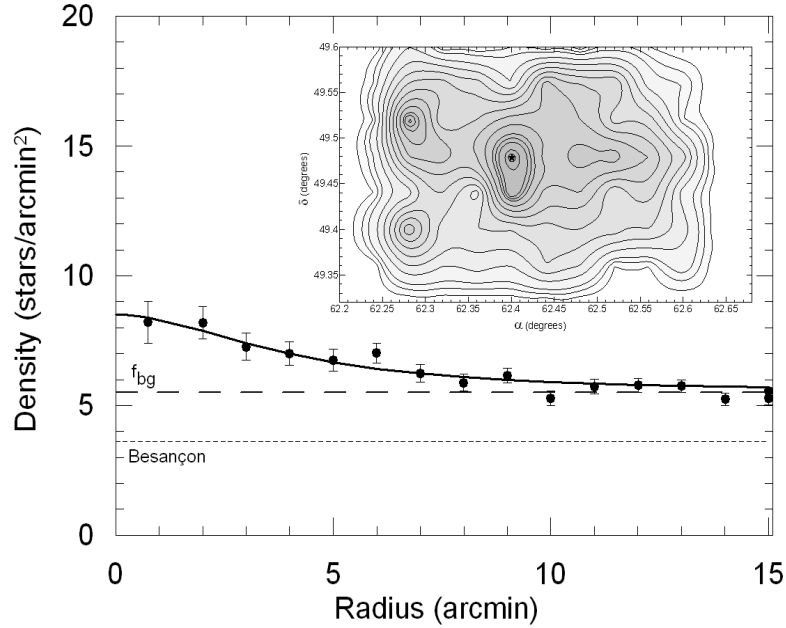


Fig. 6 Radial surface distribution of NGC 1513. *Dots*: Observational data, *solid line*: King profile, *dashed line*: Number of background stars calculated using Besançon galaxy model, *thick dashed line*: Number of observational background stars. Errors are determined from sampling statistics ($1/\sqrt{N}$ where N is the number of stars used in the density estimation at that point). The contour map in the upper right shows how we determined the centre of the cluster. The star symbol in the upper right represents the centre.

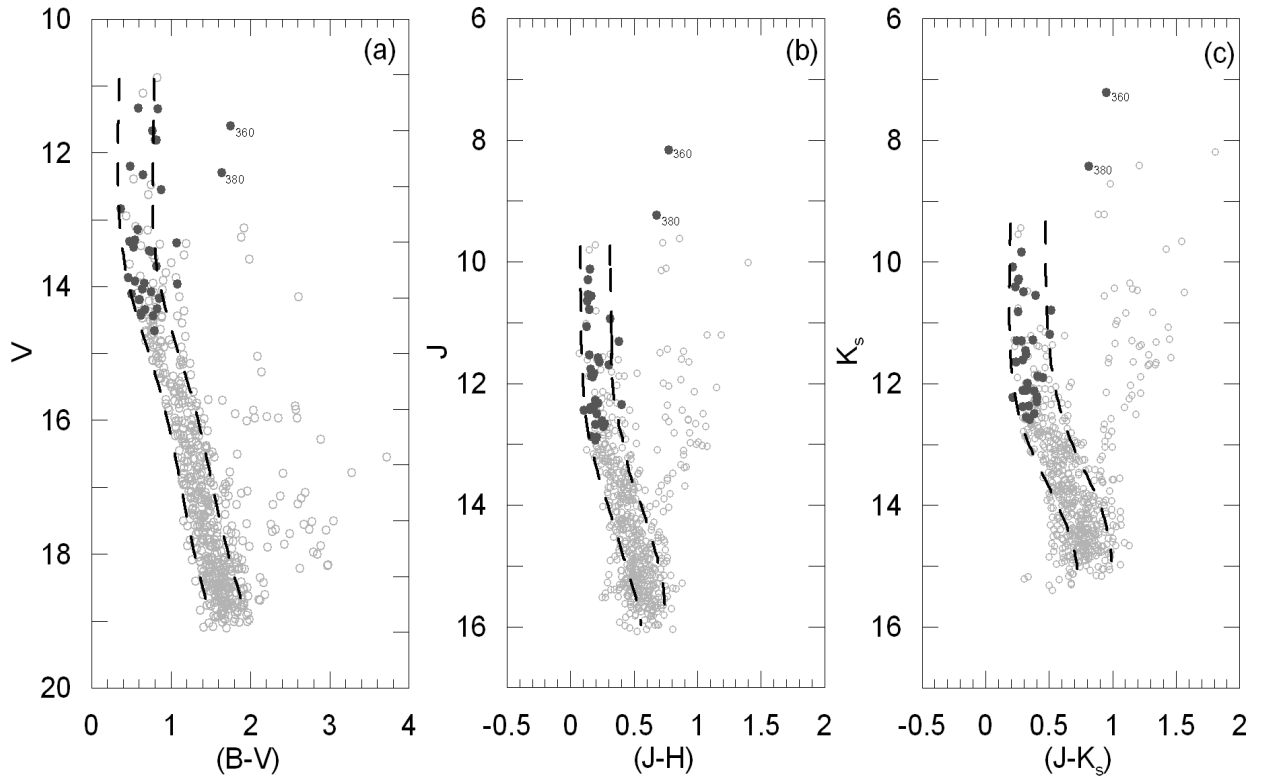


Fig. 7 Optical and near-infrared colour-magnitude diagrams for NGC 1513. Empty circles and filled circles denote the stars in this study and Frolov et al.'s (2002) high probability cluster stars, respectively. The dashed lines were obtained using the cluster members with $r \leq 5$ arcmin, while the stars in-between the lines have $r \leq 15$ arcmin.

The stars numbered 360 and 380 are also shown in all panels.

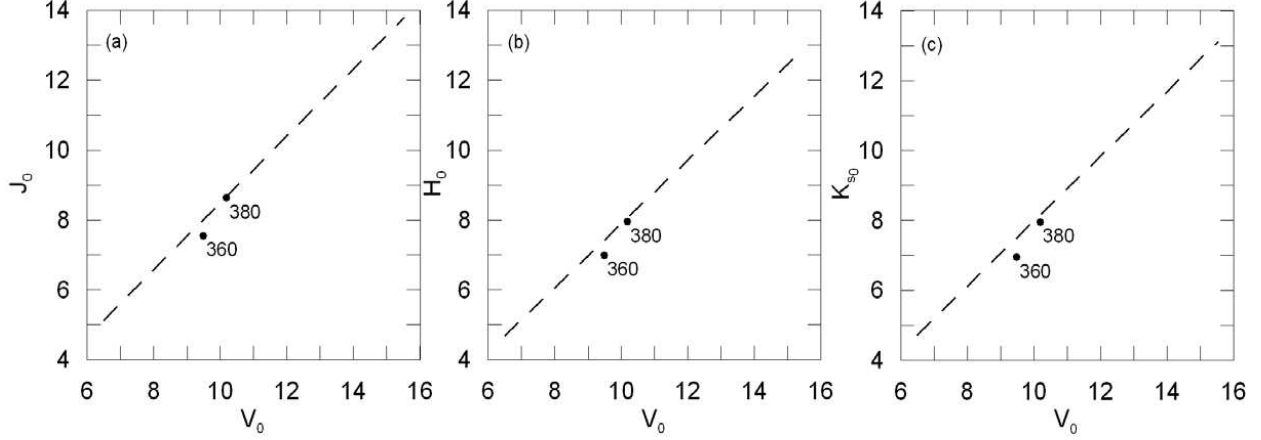


Fig. 8 The stars numbered 360 and 380 in magnitude-magnitude diagrams. The dashed lines represent the border of giant/dwarf separation. (a) V_0/J_0 , (b) V_0/H_0 , (c) $V_0/(K_s)_0$.

Table 4 Pickles' (1998) original synthetic colours (1-5). $(J - H)$ and $(J - K_s)$ were calculated using Carpenter's (2001) transformation equations (6-7).

SpType	Pickles' colours				2MASS	
	(1) $(B - V)$	(2) $(V - J)$	(3) $(V - H)$	(4) $(V - K)$	(5) $(J - H)$	(6) $(J - K_s)$
O5V	-0.380	-0.737	-0.992	-1.096	-0.202	-0.214
O9V	-0.331	-0.718	-0.899	-0.989	-0.182	-0.194
B0V	-0.342	-0.695	-0.834	-0.856	-0.163	-0.175
B1V	-0.244	-0.632	-0.732	-0.780	-0.143	-0.145
B3V	-0.201	-0.482	-0.734	-0.798	-0.123	-0.115
B5-7V	-0.139	-0.322	-0.370	-0.395	-0.094	-0.076
B8V	-0.109	-0.229	-0.259	-0.283	-0.074	-0.046
B9V	-0.044	-0.141	-0.147	-0.160	-0.055	-0.027
A0V	0.015	0.003	0.000	-0.009	-0.045	-0.017
A2V	0.029	-0.017	-0.149	-0.136	-0.035	0.003
A3V	0.089	0.036	-0.129	-0.126	-0.016	0.032
A5V	0.153	0.288	0.351	0.360	0.014	0.062
A7V	0.202	0.369	0.459	0.474	0.043	0.101
F0V	0.303	0.533	0.663	0.683	0.082	0.140
F2V	0.395	0.607	0.621	0.645	0.122	0.190
F5V	0.458	0.827	1.030	1.058	0.180	0.248
F6V	0.469	0.900	1.110	1.128	0.210	0.288
F8V	0.542	1.012	1.219	1.245	0.249	0.317
G0V	0.571	1.017	1.275	1.300	0.298	0.376
G5V	0.686	1.190	1.452	1.507	0.288	0.386
K2V	0.924	1.650	2.142	2.226	0.445	0.563
K3V	0.930	1.808	2.366	2.396	0.484	0.612
K4V	1.085	1.973	2.541	2.643	0.523	0.661
K5V	1.205	2.172	2.770	2.872	0.553	0.691
K7V	1.368	2.398	2.968	3.094	0.602	0.779
M0V	1.321	2.855	3.514	3.678	0.612	0.809
M1V	1.375	2.974	3.622	3.896	0.602	0.909
M2V	1.436	3.294	3.961	4.139	0.602	0.829
M3V	1.515	3.817	4.449	4.674	0.582	0.839
M4V	1.594	4.422	5.038	5.306	0.563	0.860
M5V	1.663	5.253	6.096	6.393	0.563	0.920
M6V	1.816	6.362	7.026	7.409	0.602	1.008

4 and our observations in two-colour diagrams (Fig. 9). In order to determine the reddening we calculated loci (represented by star symbols in Fig. 9) for our observational data and plot the best fit for those loci. These loci represent the main-sequence for our observations and we slide that main-sequence in both directions until it fits best with the standard main-sequence. The amount of sliding gives us the colour excesses for Fig. 9a and b, $E(J - H)$, $E(B - V)$ and $E(J - K_s)$, $E(B - V)$ respectively. The colour excesses and their relative errors we obtained using minimum χ^2 method are as follows: $E(J - H) = 0.21 \pm 0.02$, $E(B - V) = 0.68 \pm 0.06$ and $E(J - K_s) = 0.33 \pm 0.04$, $E(B - V) = 0.68 \pm 0.06$ mag, respectively. The confidence level of colour excess errors is 99.5%. The contour maps of two-colour diagrams in Fig. 10 show the optimum colour excesses for BV and 2MASS photometries.

Del Rio & Huestamendia (1988) obtained RGU colour excess as $E(G - R) = 0.94$ mag from standard stars. Frolov et al. (2002) converted this value into $E(B - V)$ using Steinlin's (1968) formula and calculated $E(B - V) = 0.67$ mag. The recent study of Maciejewski & Niedzielski (2007) estimates $E(B - V) = 0.76^{+0.13}_{-0.18}$ mag. Obviously, our value is almost in perfect agreement with Frolov et al.'s (2002), whereas Maciejewski & Niedzielski's (2007) agrees only within error bars.

Fiorucci & Munari (2003) calculated the colour excess values for 2MASS photometric system. According to them the colour excess ratios are: $E(J - H)/E(B - V) = 0.322 \pm 0.074$ and $E(J - K_s)/E(B - V) = 0.505 \pm 0.053$ mag. We ended up with the following results: $E(J - H)/E(B - V) = 0.309 \pm 0.130$ and $E(J - K_s)/E(B - V) = 0.485 \pm 0.150$ mag. The results produced for normal interstellar medium by

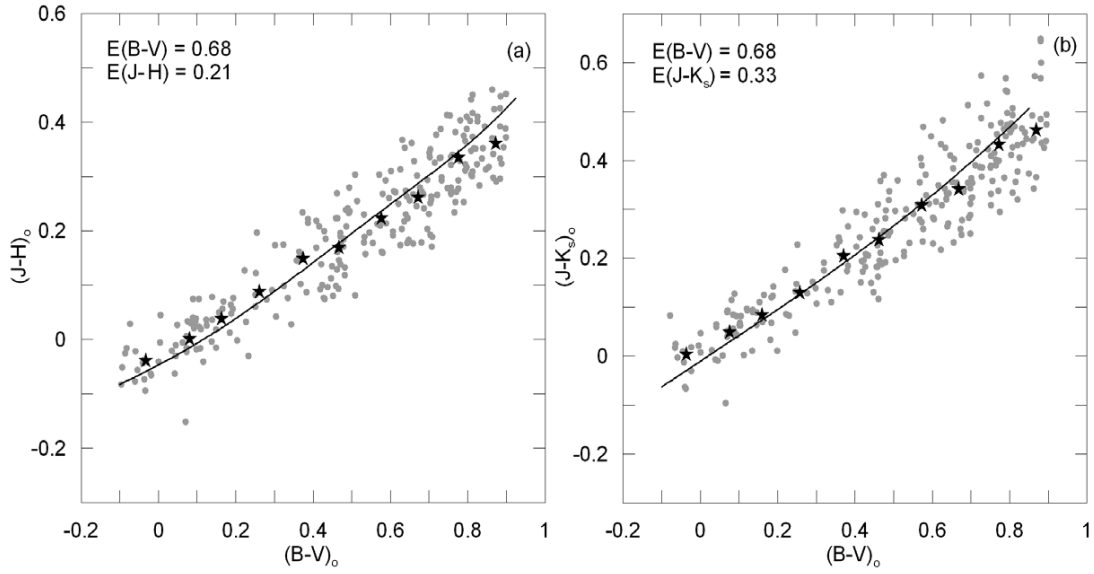


Fig. 9 Optical and near-infrared two-colour diagrams. Filled circles, the solid line and star symbols represent stars within $r \leq 5$ arcmin angular separation from the cluster centre, Pickles' (1998) original synthetic main-sequences and the loci of the main-sequence stars for the cluster, respectively.

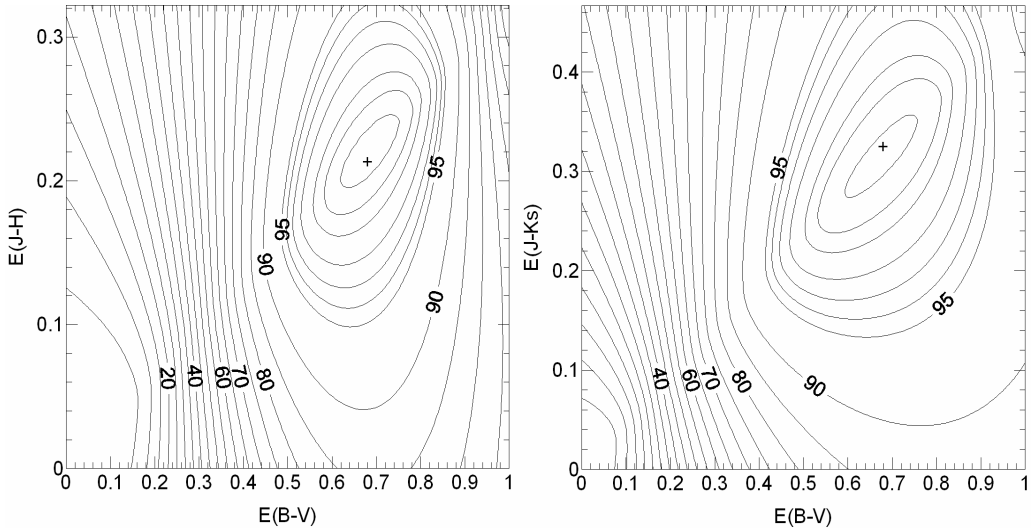


Fig. 10 Colour excess diagrams. The plus symbol represents the reduced minimum χ^2 in both panels, whereas the contours denote the probability distribution of reduced χ^2 . These contours are used in determining the colour excesses and their relative errors.

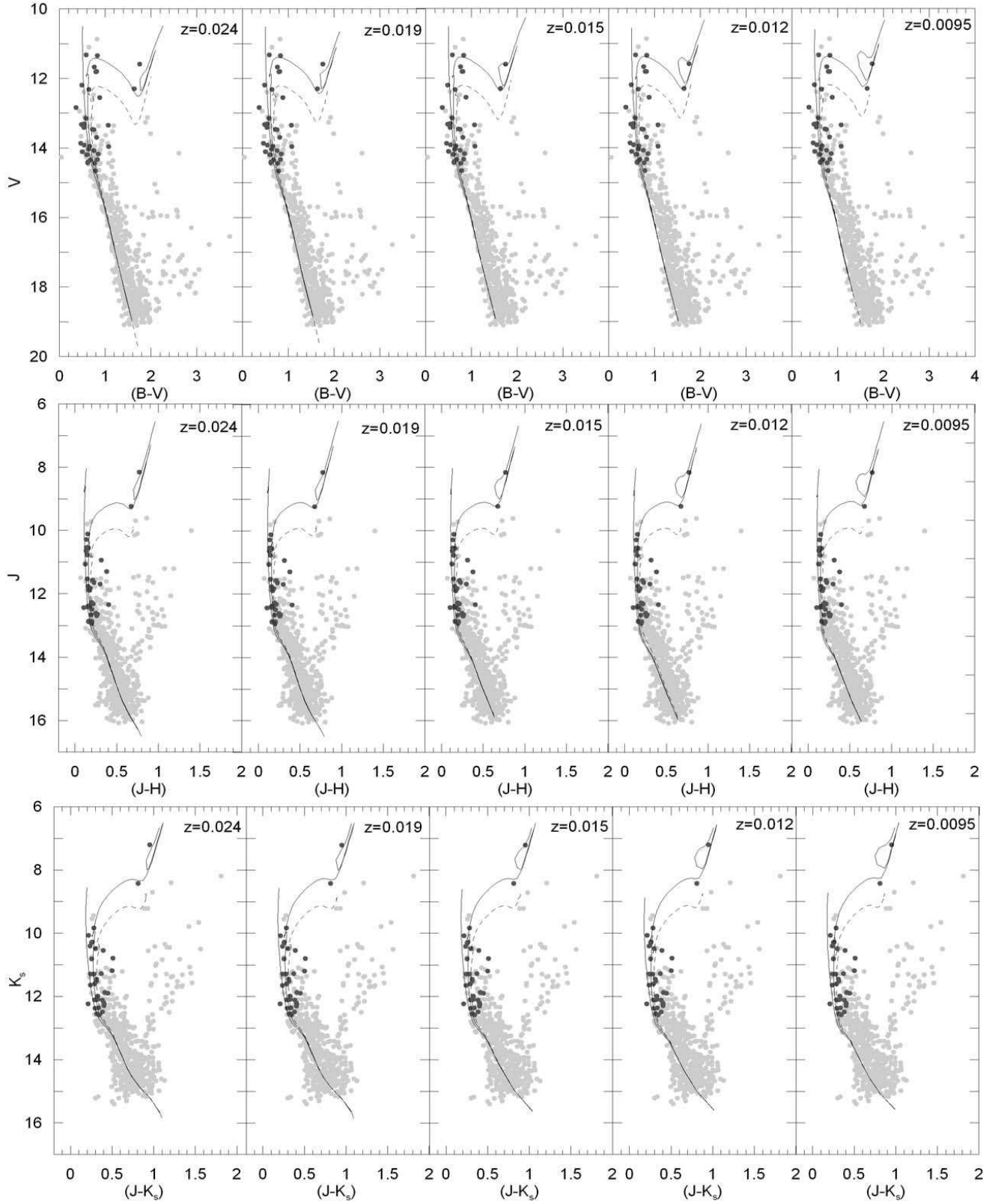


Fig. 11 $V/(B - V)$, $J/(J - H)$ and $J/(J - K_s)$ CMDs of the cluster. The black circles represent high probability ($P > 50\%$) cluster members; whereas the grey circles denote the low probability cluster members and field stars. Thin solid line: ZAMS, thick solid curve line: $\log(t/yr) = 8.40$, thin dashed curve line: $\log(t/yr) = 8.60$.

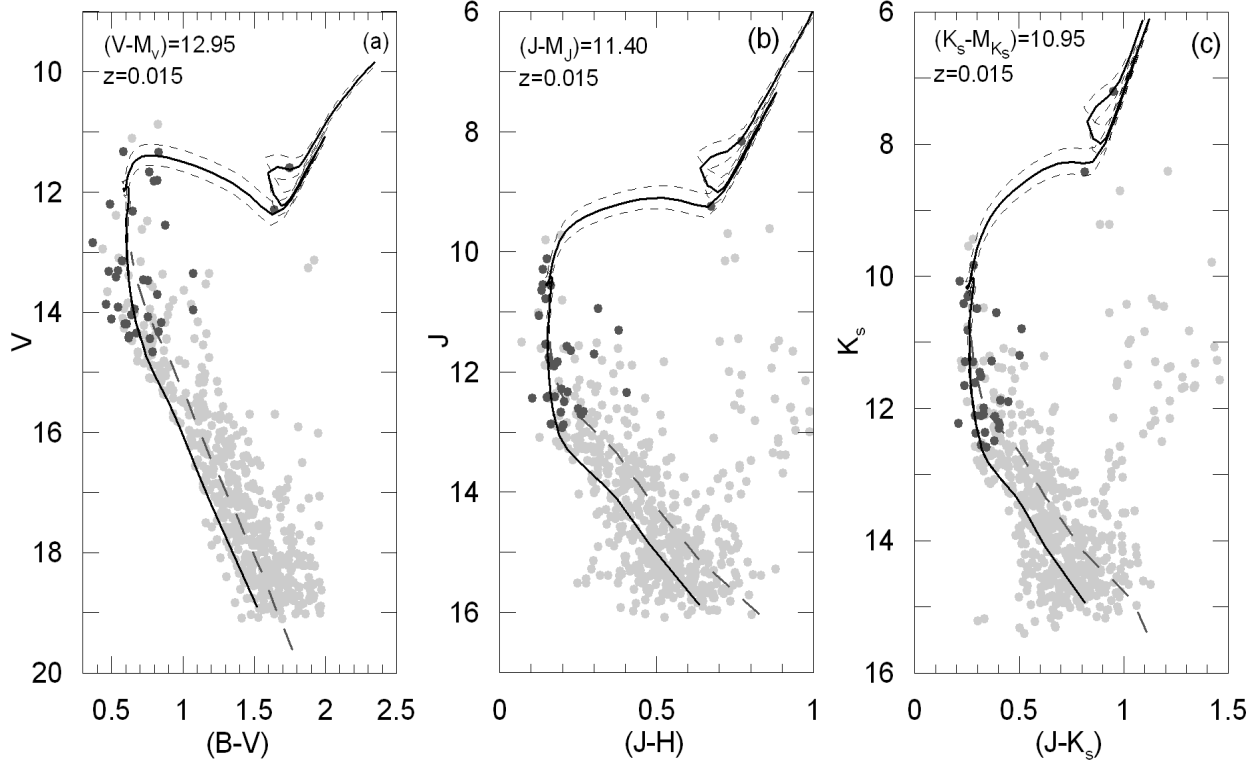


Fig. 12 $V/(B-V)$, $J/(J-H)$ and $J/(J-K_s)$ CMDs of the cluster. The solid, dashed upper and lower curves correspond to $\log(t/yr) = 8.40$, $\log(t/yr) = 8.35$ and $\log(t/yr) = 8.44$ isochrones, respectively. Finally, the thick-dashed line stands for binary sequence.

Fiorucci & Munari (2003) is in agreement with our results.

3.4 Distance and Age of the Cluster

The zero age main-sequence (ZAMS) fitting procedure was used to derive the distance to the cluster. We added Schmidt-Kaler’s (1982) ZAMS to the optical CMDs in Fig. 11. We used the colour excess $E(B-V) = 0.68$ mag discussed in Section 3.3 and reddened Schmidt-Kaler’s (1982) ZAMS accordingly. We slid the cluster’s main-sequence vertically until it overlapped with the Schmidt-Kaler (1982) one. The distance modulus of the cluster is the amount of sliding we have applied to the cluster’s main-sequence, which is $(V-M_V) = 12.95$ mag. Since there is no 2MASS data regarding Schmidt-Kaler’s (1982) ZAMS, we have selected proper 2MASS data from the Padova isochrones⁴ with solar metallicity. We plotted 2MASS ZAMS (Marigo et al. 2008) in Fig. 11. Then, we applied the previous procedure to 2MASS CMDs (Fig. 11) using reddening values of $E(J-H) = 0.21$ and $E(J-K_s) = 0.33$ mag. The optical and near-infrared ZAMS are given as thin solid lines

in all panels of Fig. 11. Finally, we calculated the distance moduli for $J/(J-H)$ and $K_s/(J-K_s)$ diagrams and obtained $(J-M_J) = 11.40$ and $(K_s-M_{K_s}) = 10.95$ mag, respectively. To de-redden the distance moduli calculated from CMDs, we used Fiorucci & Munari’s (2003) formulae: $A_V = 3.1 \times E(B-V)$, $A_J = 0.887 \times E(B-V)$, $A_{K_s} = 0.322 \times E(B-V)$ and obtained: $(V-M_V)_0 = 10.84 \pm 0.19$, $(J-M_J)_0 = 10.80 \pm 0.10$ and $(K_s-M_{K_s})_0 = 10.73 \pm 0.10$ mag, using these de-reddened distance moduli we obtained the distance of NGC 1513 1472, 1445 and 1400 pc, respectively. These results, obtained from two different photometric systems, are of $\pm 5\%$ relative difference with each other. Moreover, both Frolov et al. (2002) and Maciejewski & Niedzielski (2007) calculated the distance of the cluster as 1320 pc, which indicates a relative difference of $\simeq 10\%$.

The age of a star cluster can be determined by comparing the observed CMDs with theoretical isochrones. To determine the age of a cluster colour excess, distance modulus and metallicity needs to be known. In this study, we determined the colour excess and distance modulus, separately. However, since there is no spectroscopic data regarding the NGC 1513 its metallicity remains unknown. Hence, we took into account the

⁴<http://stev.oapd.inaf.it/cgi-bin/cmd>

metallicity during the calculation of the age by using a set of isochrones for stars with masses $0.15 < M_{\odot} \leq 100$, different metal abundance $0.0001 \leq Z \leq 0.03$ and ages from $\log(t/yr) < 10.24$ published on the web site of the Padova research group and described in the work of Marigo et al. (2008). We produced several isochrones for optical and near-infrared bands with different metal abundances ranging from 0.0095 to 0.024, which corresponds to $[M/H] = -0.30$ and $[M/H] = 0.10$ dex, respectively (solar abundance was assumed as $Z_{\odot} = 0.019$). The CMDs and the isochrones are given in Fig. 11. On each CMD, we plotted three isochrones representing three different ages: ZAMS, $\log(t/yr) = 8.40$, $\log(t/yr) = 8.60$. As seen from Fig. 11, the isochrones with $Z = 0.015$ provide the best fit for the cluster's main-sequence, main-sequence turn-off point and giant stars. Therefore, we assumed $Z = 0.015$ (corresponds to a metallicity of $[M/H] = -0.10$ dex) to be the metal abundance of the cluster.

To determine the age precisely, we plotted three isochrones with ages $\log(t/yr) = 8.35$, $\log(t/yr) = 8.40$ and $\log(t/yr) = 8.44$ in the CMDs with $Z = 0.015$ (Fig. 12). The isochrone with $\log(t/yr) = 8.40$ seemed to represent the cluster best, because it fits with both the main-sequence and the giants of the cluster. The loop (Fig. 12a: $B - V = 0.61$, $V = 11.93$; Fig. 12b: $J - H = 0.16$, $J = 10.44$; Fig. 12c: $J - K_s = 0.26$, $K_s = 10.05$ mag) in the $\log(t/yr) = 8.40$ isochrone marks the ending of hydrogen burning in the core, compression of the core and hydrogen burning in the thick layer. The star numbered 380 is located almost at the base of the red giant branch, and the star numbered 360 at the stage of helium burning. The turn-off point of the main-sequence corresponding to this isochrone is $(B - V)_0 = -0.11$ mag, which is the colour index for the B8 spectral type. To determine the binary effect regarding the cluster, we assumed the stars in the cluster to be binary systems of equal-massed components. In this case, absolute magnitude is 0.75 mag brighter than it should normally be. This binary main-sequence with $\log(t/yr) = 8.40$ has been plotted in Fig. 12 as a thick-dashed line.

Consequently, the average distance of the cluster is $d = 1440 \pm 80$ pc, the metallicity $Z = 0.015 \pm 0.004$ ($[M/H] = -0.10 \pm 0.10$ dex) and average age is $\log(t/yr) \sim 8.40$. These results partially agree with Frolov et al.'s (2002) results. They determined the distance, metallicity and average age as $d = 1320$ pc, $Z = 0.019$ ($[M/H] = 0$ dex) and $\log(t/yr) = 8.40$. Comparing our results with Frolov et al.'s (2002), we can claim that the distance we calculated is within 10% of each other, while the metallicity seems lower and age is the same. Maciejewski & Niedzielski (2007) estimated

the age of the cluster $\log(t/yr) = 7.4$, which is not in agreement with the age we calculated, which might be due to the fact that they did not take the giant stars of the cluster into account. To determine the integrated absolute magnitudes and colours of NGC 1513 in optical and near-infrared, we used Lata et al.'s (2002) equations and obtained the following results for cluster stars ($r \leq 5$ arcmin): $I(M_V) = -2.136$, $I(B - V)_0 = 0.032$, $I(J - H)_0 = 0.053$ and $I(J - K_s)_0 = -0.037$ mag. According to Table 4 the optical integrated colour corresponds to A2 spectral type.

4 Conclusion

We present CCD BV and JHK_s 2MASS photometric data for the low central concentration young star cluster NGC 1513. The results obtained in the analysis are the following:

i) We determined the centre of the cluster as $\alpha_{2000} = 04^h 09^m 36^s$, $\delta_{2000} = 49^{\circ} 28' 43''$ and its galactic coordinates $l = 152^{\circ}.57$, $b = -1^{\circ}.64$. The radial density profile shows that the angular radius of the cluster is $r = 10$ arcmin.

ii) The optical and near-infrared colours of the cluster main-sequence reveal the colour excesses, $E(B - V) = 0.68 \pm 0.06$, $E(J - H) = 0.21 \pm 0.02$ and $E(J - K_s) = 0.33 \pm 0.04$ mag. We estimated $E(J - H)/E(B - V) = 0.309 \pm 0.130$ and $E(J - K_s)/E(B - V) = 0.485 \pm 0.150$ mag.

iii) We compared the optical main sequence of the cluster with Schmidt-Kaler's (1982) ZAMS, the near-infrared one with Padova isochrones' ZAMS (Marigo et al. 2008). We obtained the distance moduli as $(V - M_V)_0 = 10.84 \pm 0.19$ for optical colour and $(J - M_J)_0 = 10.80 \pm 0.10$, $(K_s - M_{K_s})_0 = 10.73 \pm 0.10$ mag for near-infrared colours. The average distance derived from these moduli is 1440 ± 80 pc.

iv) The Padova isochrone with $Z = 0.015$ and $\log(t/yr) = 8.40$ provides the best fit for the cluster in both optical and near-infrared CMDs. Therefore, we conclude that the cluster is $\log(t/yr) = 8.40 \pm 0.04$ and has a metallicity of $[M/H] = -0.10 \pm 0.10$ dex.

5 Acknowledgements

We thank to TÜBİTAK for a partial support in using RTT150 (Russian-Turkish 1.5-m telescope in Antalya) with project number TUG-RTT150.04.016. The anonymous referee's contributions towards the paper helped us improve it. We would also like to thank Dr. Funda Güver and Astronomer Hikmet Çakmak for their contributions. This research has made use of the WEBDA

database, operated at the Institute for Astronomy of the University of Vienna. This research has made use of the SIMBAD database, operated at CDS, Strasbourg, France. This publication makes use of data products from the 2MASS, which is a joint project of the University of Massachusetts and the Infrared Processing and Analysis Center/California Institute of Technology, funded by the National Aeronautics and Space Administration and the National Science Foundation.

References

- Barhatova, K. A., Drjakhlushina, L. I., 1960, *Astronomicheskii Zhurnal* 37, 332
- Bilir, S., Karaali, S., Güver, T., Karataş, Y., Ak, S. 2006, *AN* 327, 72
- Bilir, S., Cabrera-Lavers, A., Karaali, S., Ak, S., Yaz, E., Lopez-Corredoira, M., 2008, *PASA* 25, 69,
- Bronnikova, N. M., 1958a, *Izv. Glav. Astron. Obs. Pulkovo* No. 161, 144
- Bronnikova, N. M., 1958b, *Trudy Glav. Astron. Obs. Pulkovo Ser. 2*, 72, 79
- Carpenter, J. M., 2001, *AJ* 121, 2851
- Cutri, R. M., et al., 2003, *2MASS All-Sky Catalog of Point Sources*, CDS/ADC Electronic Catalogues 2246
- Del Rio, G., Huestamendia, G., 1988, *A&AS* 73, 425
- Fiorucci, M., Munari, U., 2003, *A&A* 401, 781
- Frandsen, S., Arentoft, T., 1998, *A&A* 333, 524
- Frolov, V. N., Jilinski, E. G., Ananjevskaja, J. K., Poljakov, E. V., Bronnikova, N. M., Gorshanov, D. L., 2002, *A&A* 396, 125
- King, I., 1966, *AJ* 71, 64
- Lata, S., Pandey, A. K., Sagar, R., Mohan, V., 2002, *A&A* 388, 158
- Maciejewski, G., Niedzielski, A., 2007, *A&A* 467, 1065
- Marigo, P., Girardi, L., Bressan, A., Groenewegen, M. A. T., Silva, L., Granato, G. L., 2008, *A&A* 482, 883
- Pickles, A. J., 1998, *PASP* 110, 863
- Robin, A. C., Reylé, C., Derrière, S., Picaud, S., 2003, *A&A* 409, 523
- Schmidt-Kaler, T., 1982, *Bull. Inf. Centre Donnees Stellaires* 23, 2
- Skrutskie, M. F., et al., 2006, *AJ* 131, 1163
- Steinlin, U. W., 1968, *Zeitschrift für Astrophysik* 69, 276
- Stetson, P. B., 1987, *PASP* 99, 191
- Stetson, P. B., 1992, *Astronomical Data Analysis Software and Systems I*, A.S.P. Conference Series, Vol. 25, eds. Diana M. Worrall, Chris Biemesderfer, and Jeannette Barnes, p. 297